Ambient-pressure CVD of graphene on low-index Ni surfaces using methane: A combined experimental and first-principles study

Daniela L. Mafra,[1] Jimena A. Olmos-Asar,[2,3,*] Fabio R. Negreiros,[2,3,†] Alfonso Reina,[4] Ki Kang Kim,[5] Mildred S. Dresselhaus,[1,6] Jing Kong,[1] Gary J. Mankey,[7,8] and Paulo T. Araujo[7,8,9,‡]

[1]*Department of Electrical Engineering and Computer Sciences, Massachusetts Institute of Technology, Cambridge, Massachusetts 02139, USA*

[2]*Centro de Ciências Naturais e Humanas, Universidade Federal do ABC, Santo André, 09210-580 SP, Brazil*

[3]*INFIQC, CONICET, Departamento de Química Teórcia y Computacional, Facultad de Ciencias Químicas, Universidad Nacional de Córdoba, X5000HUA, Argentina*

[4]*Department of Materials Science and Engineering, Massachusetts Institute of Technology, Cambridge, Massachusetts 02139, USA*

[5]*Department of Energy and Materials Engineering, Dongguk University-Seoul, Seoul, 04620, Republic of Korea*

[6]*Department of Physics, Massachusetts Institute of Technology, Cambridge, Massachusetts 02139, USA*

[7]*Department of Physics and Astronomy, The University of Alabama, Tuscaloosa, Alabama 35487, USA*

[8]*Center for Materials for Information Technology (MINT Center), The University of Alabama, Tuscaloosa, Alabama 35401, USA*

[9]*Natural Sciences Institute, Graduate Program in Physics - Federal University of Para, Belem, PA 66075-110, Brazil*

(Received 1 April 2018; published 23 July 2018)

The growth of large area single-layer graphene (1-LG) is studied using ambient pressure chemical vapor deposition on single-crystal Ni(111), Ni(110), and Ni(100). By varying both the furnace temperature in the range of 800–1100 °C and the gas flow through the growth chamber, uniform, high-quality 1-LG is obtained for Ni(111) and Ni(110) single crystals and for Ni(100) thin films. Surprisingly, only multilayer graphene growth could be obtained for single-crystal Ni(100). The experimental results are analyzed to determine the optimum combination of temperature and gas flow. Characterization with optical microscopy, Raman spectroscopy, and optical transmission support our findings. Density-functional theory calculations are performed to determine the energy barriers for diffusion, segregation, and adsorption, and model the kinetic pathways for formation of different carbon structures on the low-index surfaces of Ni.

DOI: 10.1103/PhysRevMaterials.2.073404

I. INTRODUCTION

The growth of carbon structures on different metallic/semimetallic substrates has been extensively studied in the past decades [1–50]. Much of this research has focused on the formation of graphene on low-index nickel single-crystal surfaces, Ni(111), Ni(110), and Ni(100) [1–27,43–46]. However, a complete microscopic understanding of the thermodynamic pathways for graphene formation on these surfaces is still lacking [15,16,30,31,46,47,51–57]. The growth of single-layer graphene (1-LG) on Ni(111) and Ni(110) surfaces has been reported, but similar explanations for the growth mechanisms on both surfaces is given. These explanations do not account for the distinctly different thermodynamic properties of the fcc (111) and (110) surfaces [1–27,30,31,43–47,51–57]. Advances in 1-LG growth techniques have been boosted by the isolation of 1-LG from bulk graphite substrates [28], and recent research has shown the possibility of growing 1-LG and multilayer graphene (M-LG) on metals using chemical vapor deposition (CVD) techniques without the added difficulty of ultrahigh vacuum environments and the subsequent transfer of such a material to dielectric substrates [7–19,29–32,54–57]. The combination of process flexibility and high quality of the material produced from these fabrication processes has enabled the integration of graphene into various applications [33,43–47,51–57].

Although graphene has been grown successfully on a wide range of transition metals, copper and nickel are the most widely used substrates [9,43–47,51–57]. Copper is the most frequently used metal to grow monolayer graphene, since the low carbon solubility in Cu leads to a desirable self-limiting surface growth of graphene [19,32]. The same is not true for nickel (Ni), because the high bulk solubility of carbon at typical high growth temperatures can result in a high rate of carbon segregation and subsequent M-LG formation upon cooling. The growth of 1-LG on Cu, in general, needs to be carried out under low pressure [34], further complicating the synthesis process and adding to the cost of graphene production. The advantage to using nickel is that the growth of M-LG can be avoided by selecting the proper growth conditions. Due to a stronger interaction between graphene and Ni, only one graphene domain orientation exists for growth on Ni(111) single crystals. So in this case, no tilt-grain boundaries are expected after a continuous and high-quality film of graphene is formed [35].

The formation mechanisms of 1-LG are different for Cu and Ni. Growth of 1-LG in Cu is mainly mediated by the

*Corresponding author: jimenaolmos@gmail.com
†Corresponding author: f.ribeiro@ufabc.edu.br
‡Corresponding author: paulo.t.araujo@ua.edu

adsorption of carbon atoms by the surface atoms followed by the diffusion of such atoms across the surface and the formation of nucleation centers [34,43–47,51–57]. In Ni, both bulk diffusion and surface diffusion leading to the formation of nucleation centers on the surface most be considered [1–5,30,34,40,41,43–47,51–57]. The growth of 1-LG on Ni is a crucial step toward the controlled growth of high-quality multilayer graphene for a number of technological applications [43–47,51–57]. This motivates our study in order to further optimize the growth conditions by building on the work of Seah *et al.*, who demonstrated the growth of bilayer graphene (2-LG) on Ni(111) by rapidly quenching the substrate after deposition to limit the amount of carbon segregation [56].

In this work, we show that successful growth of 1-LG via ambient pressure CVD is achieved for Ni(111) and Ni(110) single crystals and for Ni(100) thin films but only M-LG growth could be obtained for single-crystal Ni(100). We characterize the different growth mechanisms found on each orientation with optical microscopy, Raman spectroscopy, and optical transmission. Density-functional theory (DFT) calculations are performed to provide an atomistic model of the processes involved to support the experimental results. It is found that the formation of a uniform monolayer on Ni single-crystal substrates is epitaxially driven for the Ni(111) surface, while surface thermodynamic and kinetic effects drive the formation on Ni(110) and Ni(100) by diffusion and segregation of carbon atoms on Ni surfaces [2,3,5,20]. The results and explanations provided by this work are a step toward development of a means to control the number of graphene layers formed on the surface.

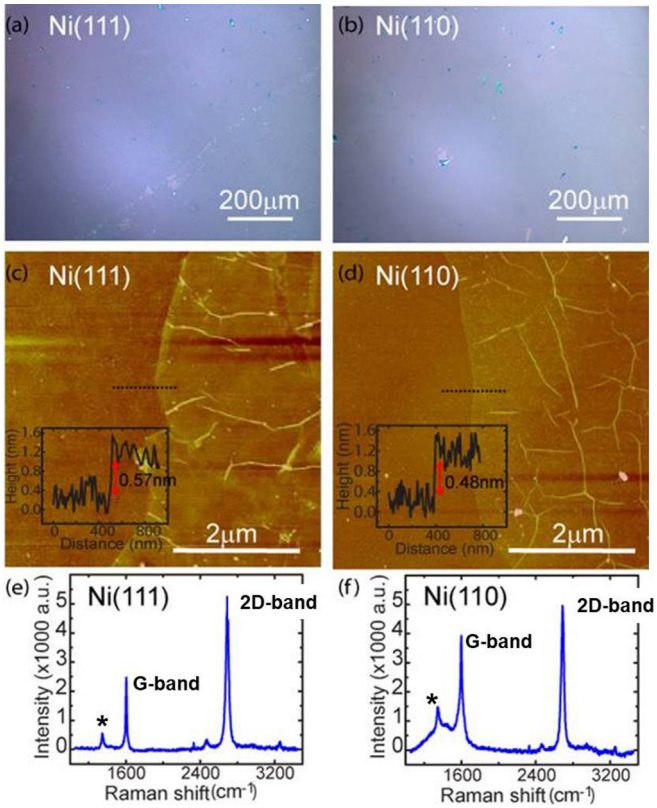

FIG. 1. Optical microscopy images of 1-LG grown on (a) Ni(111) and on (b) Ni(110) after transferring the 1-LG layer to a Si/SiO_2 substrate. AFM images of the edge of typical 1-LG films transferred to $Si\text{-}SiO_2$ for 1-LG grown on (c) Ni(111) and (d) Ni(110). The insets reveal the formation of 1-LG in each case and Raman spectra are shown for 1-LG grown on (e) Ni(111) and (f) Ni(110).

II. METHODS

A. Experimental details

The Ni(111), Ni(110), and Ni(100) single-crystal substrates used in this work (10 mm in diameter, 1 mm thick, 99.9995% purity) were obtained from Marketech International The substrates were electropolished further with a solution of glacial acetic acid and perchloric acid (60%) in the ratio of 7:3 by volume, to produce smooth substrate surfaces. x-ray diffraction measurements for each Ni substrate were performed after polishing to confirm the crystallographic orientation. The Ni(100) thin films used for the comparison study are approximately 1 mm thick. The growth of graphene was performed using an ambient pressure CVD process. A 1-inch tube furnace is initially preheated to the growth temperature before the introduction of the Ni substrates contained within an open-ended silica tube. The substrates are then precleaned by rapid heating under a flow of hydrogen at 1000 sccm. The temperature is then reduced to the growth temperature and methane gas at 100 sccm is added to the hydrogen flow. Exposure to methane continues for 300 s before removing the silica tube containing the substrates into a room-temperature environment for a fast cool down. The graphene is then transferred from the substrates using a Poly(methyl methacrylate) polymer (PMMA) layer spin coated on the surface followed by electrochemical delamination of the graphene/PMMA [[48–50]. The electrolyte consists of a 1M NaOH solution with a negative −10 V applied on the Ni. The graphene layer can then be placed on a dielectric substrate and the PMMA can be removed by immersing in acetone [17].

B. Computational details

Density-functional calculations [58] were performed with the QUANTUM-ESPRESSO package [59] and the Perdew-Burke-Ernzerhof [60] generalized gradient approximation as exchange-correlation functional. The ultrasoft pseudopotentials of the PSLIBRARY [61] were used with plane-wave/charge density energy cutoffs of 40/320 Ry. To evaluate the interaction of carbon with each Ni surface considered, the unit cells were 3×3 squares for 100, $3 \times 2\sqrt{2}$ rectangles for 110, and 3×3 hexagons for 111. The sampling of the first Brillouin zone was performed using grids centered at the Γ point, with a k-point density of $2 \times 2 \times 1$. For the graphene monolayer coverage, the unit cells of the 100/110 surfaces were increased to 4×6 and $4 \times 5\sqrt{2}$, creating an average strain in the graphene layer of less than 2%. Five Ni layers were used with additional 12 Å of vacuum in the perpendicular direction to avoid spurious interaction between periodic images. The energy and force thresholds adopted for the geometry optimizations were 0.0001/0.001 a.u., respectively, and the bottom two Ni layers were kept frozen during ionic optimizations. Van der Waals corrections within the Grimme-2D method [62] were also considered.

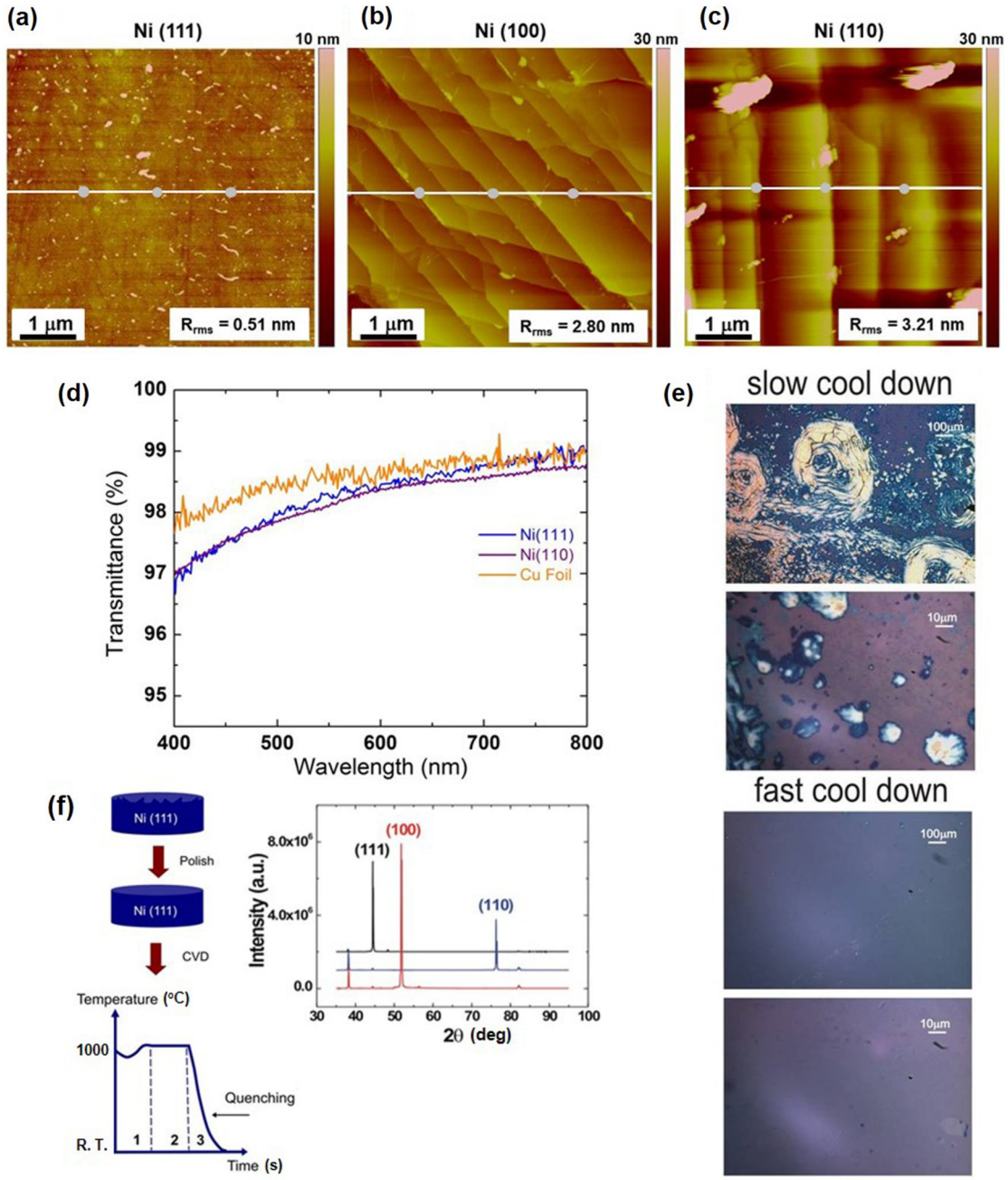

FIG. 2. Atomic force microscopy (AFM) images of clean and polished surfaces for (a) Ni(111), (b) Ni(100), and (c) Ni(110) before graphene growth. The solid lines and spaces between bullets indicate, respectively, where a surface profile line was taken and regions where roughness analyses were performed. The roughness ($R_{\rm rms}$) reported in the bottom right corner is an average of values taken in several different regions. (d) Optical transmittance across the wavelength range of 400–800 nm for 1-LG films grown on Ni(111) (blue), Ni(110) (purple), and Cu foil (orange). (e) Images of samples obtained for Ni(111) using fast and slow cool down from $T = 1000\,^{\circ}$C. Fast quenching produces a more continuous film of 1-LG, while slow quenching produces an inhomogeneous film composed of few layer flakes and fragments. (f) Schematic of the processing steps for growing 1-LG from Ni single crystal. R.T. stands for room temperature. The graphic shows the XRD measurements of the Ni(111), Ni(110), and Ni(100) single crystals.

III. RESULTS AND DISCUSSION

Figure 1 shows optical microscopy, AFM, and Raman spectroscopy characterization of the 1-LG films obtained for Ni(111) and Ni(110) after transferring the 1-LG films to Si/SiO_2 substrates [note that 1-LG in Ni(100) thin films will be discussed later in the text]. The optical images [Figs. 1(a) and 1(b)] show a uniform contrast similar to samples derived from Cu foils [17–19,23]. The observed optical color contrast corresponds to that estimated for 1-LG under the same theoretical model as was described previously [23]. The cross-sectional thickness of the film estimated from the AFM tapping mode images in within the expected values of 1-LG, ranging from 0.48–0.57 nm [Figs. 1(c) and 1(d)]. Raman spectroscopy [Figs. 1(e) and 1(f)] confirms the presence of

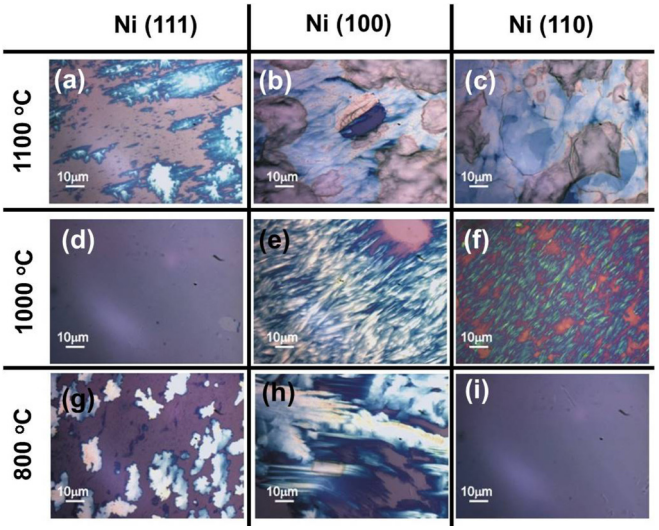

FIG. 3. Optical absorption images of graphene grown on the Ni(111), Ni(100), and Ni(110) at temperatures of 800, 1000, and 1100 °C. Multilayer graphene is obtained in all cases, except for (i) Ni(110) at 800 °C and (d) Ni(111) at 1000 °C, where 1-LG is obtained.

graphitic carbon in its monolayer configuration. Three main features are observed with 532 nm laser wavelength excitation; the D, G, and 2D Raman peaks around 1350 cm^{-1}, 1580 cm^{-1}, and 2700 cm^{-1}. The intensity ratio between the 2D and G peak intensities (I_{2D}/I_G) close to 2 and the full width at the half maximum (FWHM) of the 2D band of $\sim$30 cm^{-1} are spectroscopic signatures of the presence of 1-LG. Differences in the D-band intensity (marked with an asterisk), suggest that 1-LG grown on Ni(110) is structurally more disorganized than the corresponding film on Ni(111). Further confirmation of the presence of 1-LG and of its quality when grown on Ni(111) and Ni(110) catalysts was done by measuring the optical transmittance of the films over the visible range [Fig. 2(d)]. The films were transferred to quartz substrates and the average transmittance was measured to be approximately 97.8% for 1-LG grown on both Ni(111) and Ni(110). This value is within experimental error of the expected transmission for 1-LG of 97.7% [23]. The transmittance was also found to be nearly the same as that measured for 1-LG grown over a Cu foil following the growth process described elsewhere [36,37].

The process parameters are of significant importance for the success of 1-LG growth on Ni(111) and Ni(110) single crystals. As illustrated in Fig. 2(f), polishing the surface of Ni pieces (as described in Sec. II) was critical for 1-LG preparation due to the observed formation of M-LG under the same processing conditions on samples rougher than a few nanometers. Formation of M-LG can be attributed to the preference of graphene formation on Ni step edges, which are more abundant on rougher crystalline surfaces [25,38,39]. Growth on a rough surface results in the overlap of islands originating from neighboring step edges [1–5,35,38]. Figures 2(a)–2(c) show atomic force microscopy (AFM) images of clean and polished surfaces for Ni(111), Ni(100), and Ni(110) before graphene growth. The surface roughness is the largest for Ni(110) and the smallest for Ni(111). None of the surfaces prepared using our method were rough enough to prevent monolayer growth. In Fig. 2(f) we also show the x-ray diffraction (XRD) measurements taken from the Ni(111), Ni(110), and Ni(100) single crystals, confirming their crystallographic directions.

The cooling rate for temperature quenching of the Ni crystal plays a significant role in the crystalline structure of the resulting sample. A fast cool down prevents the formation of a graphite phase after the monolayer forms on the Ni surface [bottom panel in Fig. 2(e)]. Slow cooling results in films consisting mostly of M-LG [top panel in Fig. 2(e)]. In addition, the selected growth temperature (T) must be correct to achieve 1-LG formation on Ni. For the same gases and flow rates (H_2 = 1000 sccm, CH_4 = 100 sccm) and growth time (t = 5 min), the optimum growth temperature T depends on surface orientation. We found that 1-LG on Ni(111) is formed at $T = (1000 \pm 1)$ °C. In contrast, M-LG is formed on the Ni(110) and Ni(100) surfaces, as shown in Figs. 3(d), 3(e), and 3(f). For a growth temperature of $T = (800 \pm 1)$ °C, 1-LG is formed on Ni(110) and M-LG is formed on Ni(111) and Ni(100), as shown in Figs. 3(g), 3(h), and 3(i). For the experimental conditions investigated in this work, 1-LG was not formed on a Ni(100) single crystal, but 1-LG was formed on Ni(100) thin films. For the deposition temperatures investigated below 800 °C, no ordered carbon structures were formed on any of the Ni surfaces, independent of their crystallographic orientation. Table I summarizes the results for Ni single crystals.

A. Growth of 1-LG on Ni(111)

Nickel crystals are face centered cubic (fcc) structures with a bulk lattice parameter of 3.52 Å. Ni(111) has a surface lattice parameter of $a_{Ni(111)} = 2.49$ Å while 1-LG is a nearly perfect match with $a_{1\text{-LG}} = 2.46$ Å [1–5]. Compared to the other two orientations, Ni(110) and Ni(100), Ni(111) has the highest atomic packing density [41,63] and the smallest surface energy, $S_{Ni(111)} = 1606$ ergs cm^{-2} versus $S_{Ni(110)} = 2057$ ergs cm^{-2} and $S_{Ni(100)} = 1943$ ergs cm^{-2} [1–5,64]. Since the surface energy is related to the strength of the C-Ni interaction, we expect the carbon adsorption energy and energy barriers E_{across} for the diffusion across the surface [40–42,65] to be related to $S_{Ni(111)}$, which means that they should be lower in this (111) face. Diffusion of carbon atoms will also be dependent on its

TABLE I. Summary of the growth of carbon structures at different temperatures and different crystallographic directions using gas flow rates of 1000 sccm for H_2 and 100 sccm for CH_4. 1-LG is single-layer graphene and M-LG is multilayer graphene.

	Ni(111)	Ni(110)	Ni(100)
1100 °C	M-LG in single crystal	M-LG in single crystal	M-LG in single crystal
1000 °C	1-LG in single crystal	M-LG in single crystal	M-LG in single crystal and 1-LG in thin film
800 °C	M-LG in single crystal	1-LG in single crystal	M-LG in single crystal
750–790 °C	None	None	None

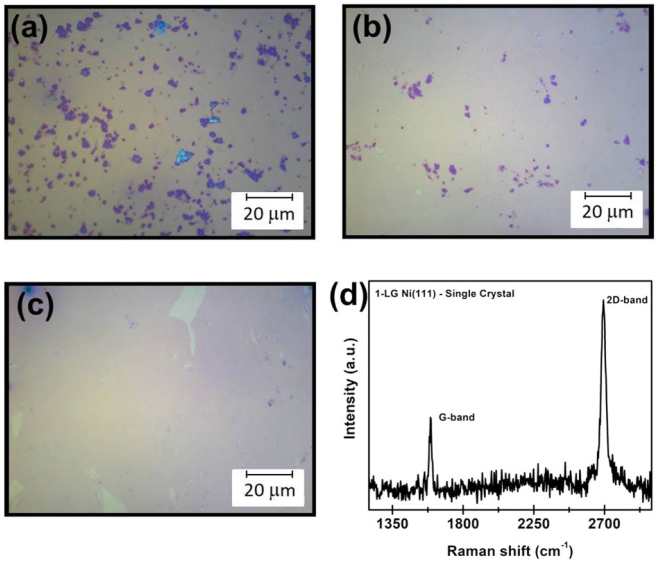

FIG. 4. Optical images of the graphene films obtained from Ni(111) at $T = 900\,^{\circ}$C and gas flows of $H_2 = 1000$ sccm and (a) $CH_4 = 100$ sccm, (b) $CH_4 = 75$ sccm and (c) CH_4 50 sccm. 1-LG is formed when the flow of methane is decreased from 100 sccm to 50 sccm. (d) Raman spectrum for the 1-LG shown in (c).

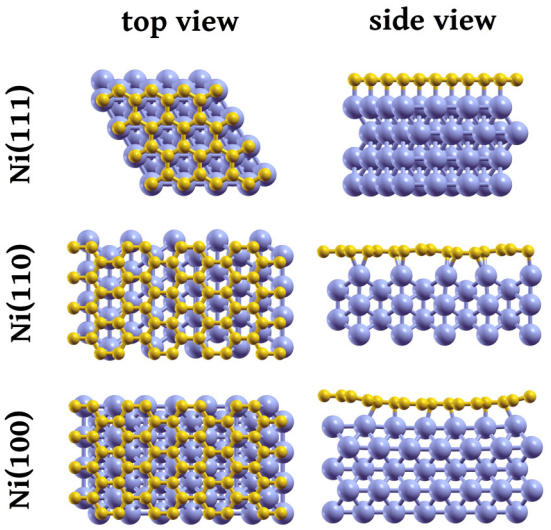

FIG. 5. 1-LG on nickel, in its optimized configuration. In yellow are carbon atoms and in blue, nickel.

surface mean-free path. If the density of C atoms increases, the mean-free path decreases, making diffusion less likely since dimers have reduced mobility. The C deposition rate is proportional to the reactivity rate of methane and is the smallest on Ni(111) at all temperatures [1–5].

For Ni(111) 1-LG was obtained at $T = (1000 \pm 1)\,^{\circ}$C, while M-LG was obtained at $T = (1100 \pm 1)\,^{\circ}$C and at $T = (800 \pm 1)\,^{\circ}$C and no carbon structure formation was observed for temperatures below $(790 \pm 1)\,^{\circ}$C (we have studied temperatures between 750 °C and 800 °C in steps of 10 °C). At the optimum growth temperature of $(1000 \pm 1)\,^{\circ}$C, the driving phenomena behind the growth are balanced, mainly the deposition rate, diffusion across the surface, diffusion into the bulk and segregation during cool down. An additional factor is that CH_4 reactivity is above a minimum threshold at this temperature, but this is already the case at 800 °C (see Table I).

At 800 °C, bulk diffusion is significantly lower compared to 1000 °C and, consequently, the segregation during the fast cool down is inhibited. Diffusion of carbon atoms into the bulk at 1000 °C and the limited segregation during rapid cooling control the density of carbon atoms for the Ni(111) surface, thereby allowing 1-LG formation. At higher temperatures such as 1100 °C, the probability of carbon atom diffusion across the surface and the probability of carbon atom diffusion into the bulk are approximately equal and the flux of carbon atoms diffusing into the bulk is larger. In addition, cooling from 1100 °C takes longer, resulting in increased carbon segregation during the cooling down process, so M-LG was preferentially obtained on Ni(111).

By changing process parameters for temperatures between 780 °C and 1000 °C, the growth of monolayers on Ni(111) is possible. Below 1000 °C, the deposition rate and the sticking coefficient of carbon on the Ni substrate decrease, so obtaining M-LG between 1000 °C and 780 °C probably means that the flow of CH_4 is still too high in such cases, even though the deposition rate decreases (diffusion into the bulk is increasingly suppressed as the temperature decreases). So by substantially decreasing the CH_4 flow, 1-LG is expected. In Figs. 4(a)–4(c), it is demonstrated that mostly 1-LG can be obtained at 900 °C if the CH_4 flow is reduced from 100 to 50 sccm, while the H_2 flow is kept at 1000 sccm and a rapid cool down is used. Figure 4(d) shows the Raman spectrum for the 1-LG grown under such conditions.

Our computer simulations suggest that 1-LG on Ni(111) has a planar structure, with half of the carbon atoms attached to an on-top position and the other half attached to a hollow-hcp position, as shown in Fig. 5. Although we present this structure as the most stable, there is still disagreement about the best atomic arrangement of graphene on Ni(111). In fact, it has been shown that more than one structure may coexist [9,66,67], due to the very low energy difference between them. The structural and energetic parameters are listed in Table II.

B. Suggested model for carbon growth on Ni(111)

We have calculated the adsorption energy of a single carbon atom on a perfect Ni(111) surface, emulating the low concentration regime, corresponding to the initial stages of growth (see Fig. 6). Nearly all generated carbon will diffuse

TABLE II. Energetic and structural information of 1-LG on different crystal planes as obtained by DFT calculations, shown in Fig. 5. The values show the average adsorption energy by atom, the average carbon-surface distance and the maximum buckling on the graphene layer.

	E_{ads}(meV.at^{-1})	$d_{graph\text{-}surf}$ (Å)	buckling (Å)
Ni(111)	164	2.11	0.00
Ni(110)	209	2.03	0.29
Ni(100)	180	2.13	0.69

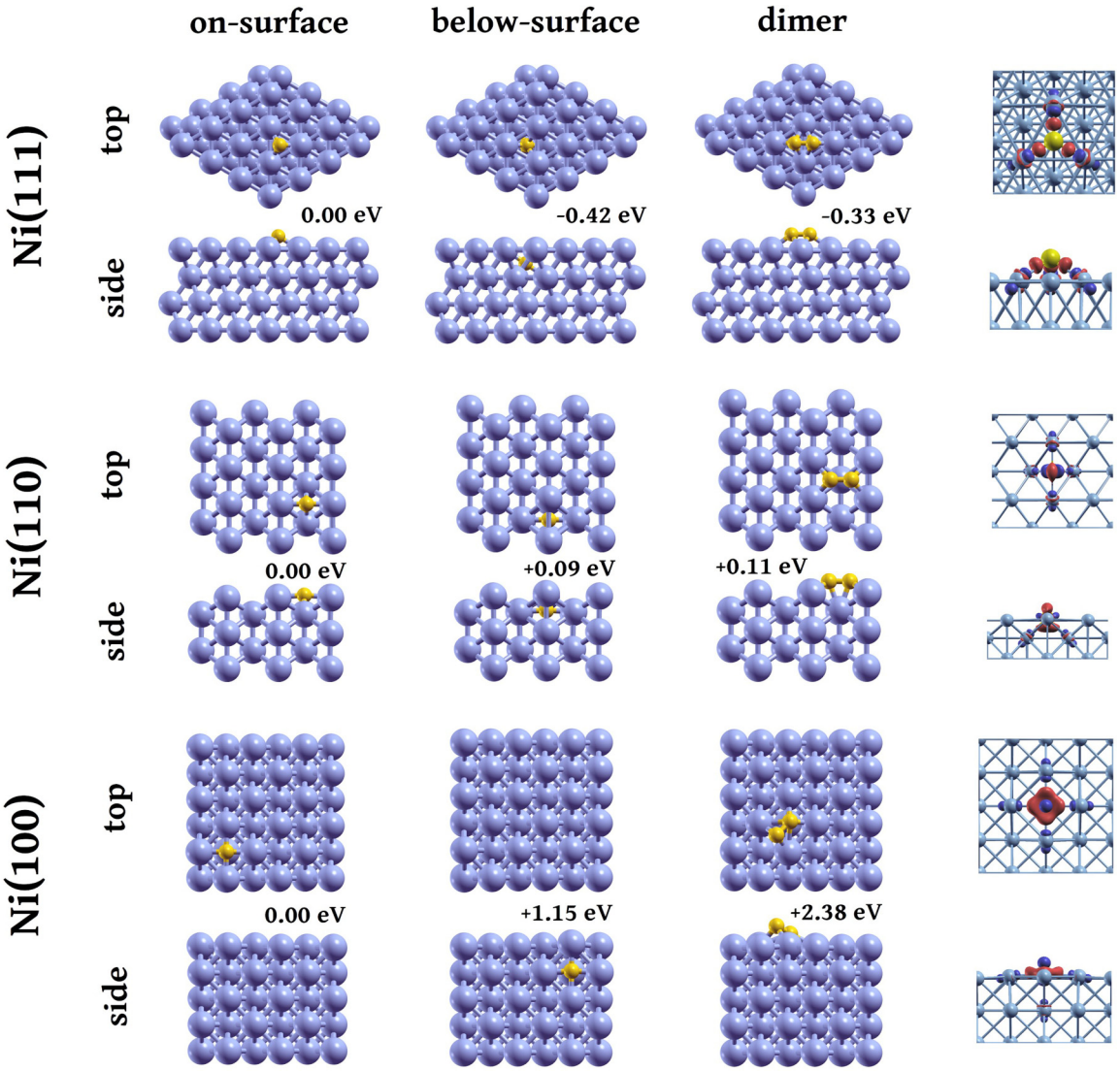

FIG. 6. The most stable sites for (from left to right): carbon adsorption, carbide formation, and dimer formation on different Ni crystal planes. The color code is the same as in Fig. 5. The relative adsorption energies for each surface are displayed, and in the case of dimers, the value corresponds to the energy variation with respect to the adsorption of two isolated C atoms. On the right, the charge density difference for single-atom adsorption is shown. In these plots, red (blue) means electron accumulation (depletion).

laterally until a dimer is formed. Trimers and tetramers are less stable than dimers, so probably the first stages of the growth will involve only dimers. The best site for carbon adsorption on the surface is on a hollow site, in agreement with theoretical results from the literature [68,69] (for more information about the structures and the way of calculating the adsorption energies, please see the Supplemental Material [70]). The carbide position, corresponding to carbon absorption is more stable by 0.42 eV. For a second C atom, there is a 0.33 eV gain in forming a dimer, instead of adsorbing far away from the first C atom. All the adsorption energies for a single carbon atom, as well as the structural parameters for the configurations, are presented in Table S1 in the Supplemental Material. To obtain an entire picture of the processes involved in the first stages of carbon deposition, we have also evaluated the diffusion barrier for diffusion across (E_{across}) and into the surface (E_{into}), as well as dimer diffusion across the surface. Figure 7(a) illustrates the main paths considered and Fig. 7(b) quantifies them, showing that E_{across} barrier is less than half of E_{into}.

With these experimental and theoretical results in mind, we propose a possible scenario for graphene formation on Ni(111). At the low coverage regime, the incoming C atoms should adsorb at the surface and diffuse across the Ni surface at a much higher rate than into the Ni bulk. If the deposition rate is large enough and the temperature is low enough to inhibit diffusion into the bulk, then the adsorbed C atoms should preferentially form dimers. Dimers are more stable than monomers, and it is nearly impossible for a dimer to diffuse into the bulk. Dimers may form trimers with incoming C atoms and the dimers can also diffuse across the surface with a somewhat higher activation energy of around 0.6 eV. Formation of a monolayer will depend mostly on a delicate balance of the deposition rate and the temperature. We also note that the formation of a carbon cluster on Ni(111) is favored by symmetry (see Fig. 6), since

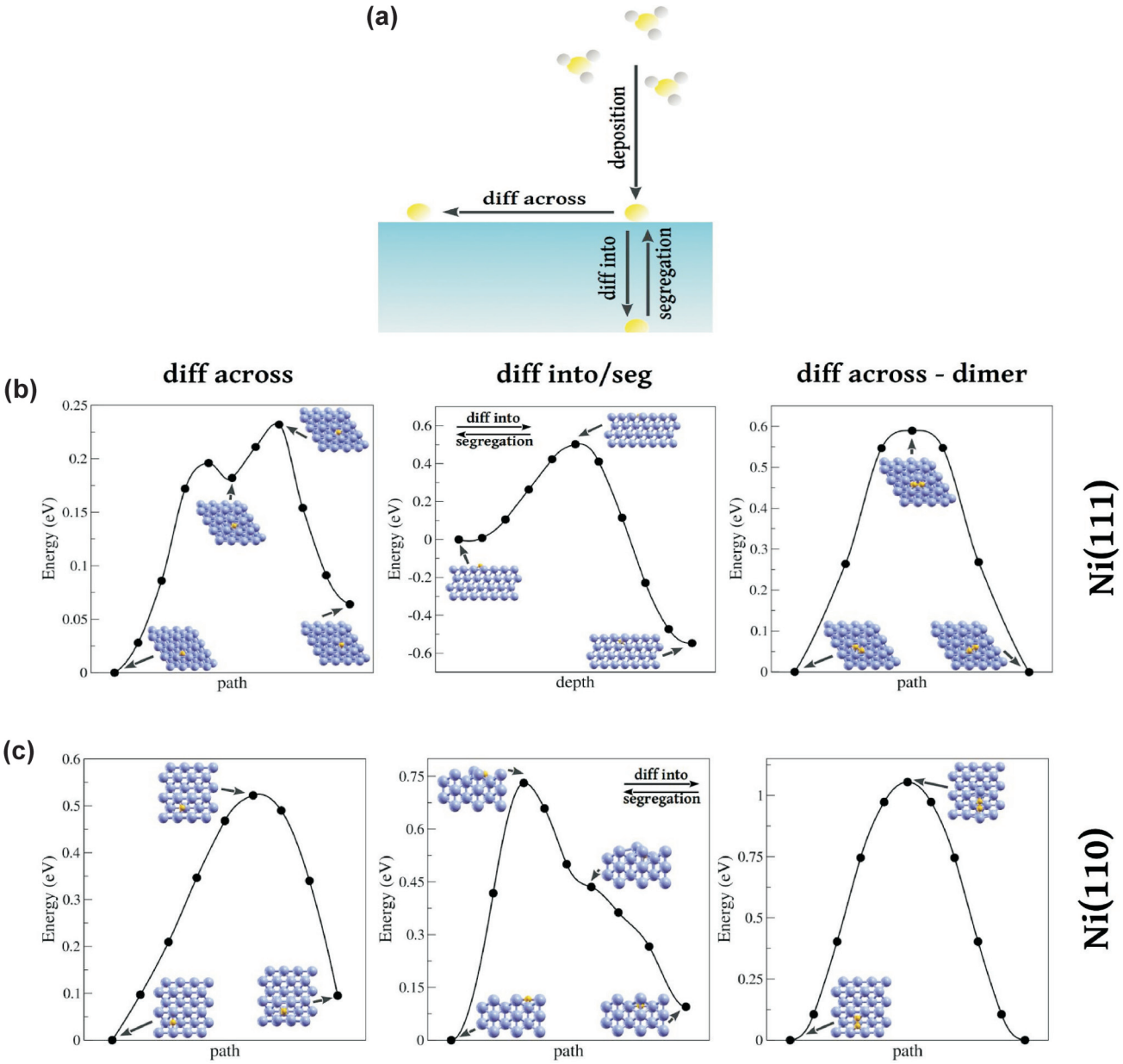

FIG. 7. Diffusion of carbon on a nickel surface. In (a) all the processes involved at the first stages of graphene growth on nickel are depicted. In (b) and (c) the kinetic barriers for diffusion across and into (or segregation, in reverse) for a single carbon atom and diffusion across for a dimer, on the 111 and 110 planes, are shown. The color code is the same as in Fig. 5. For the case of Ni(100) all the barriers are higher than 1 eV, so they are not shown.

Ni(111) has a surface with hexagonal regularity and a lattice parameter very close to that of 1-LG.

Following the work by Ozcelik [31], it is possible that the atoms attached to the edges of the clusters will form pentagons and heptagons that will grow and heal themselves forming hexagons by a Stones-Wales-Thrower mechanism. The connection among the several nucleation centers is likely to occur through this process. From these considerations, Ni(111) is expected to provide the best quality graphene. At low growth temperature (800 °C), surface diffusion of carbon atoms dominates, so eventually M-LG will grow. For higher temperatures (1000 °C), bulk diffusion dominates and less surface carbon concentration is expected. Dimer diffusion will become more probable, and dimers would connect and generate 1-LG. Finally, if the temperature is too high (1100 °C) the fast reactivity of CH_4 will generate a higher carbon concentration at the surface, so M-LG will grow. Although our calculations suggest that the growth of nucleation centers goes by the formation of dimers, the formation of nucleation centers by dimers was unclear until recently: Patera *et al.* [71] demonstrated via experiments and DFT calculations that the 1-LG growth process occurs by the addition of carbon lines parallel to the graphene edge always involving a kink site and a Ni adatom. The participation of Ni adatoms is energetically favored since it reduces the rate-limiting energy barriers by approximately 35% (according to their calculations it lowers

from 2.46 to 1.61 eV). Therefore, Ni adatoms spontaneously bind to kink sites in the graphene edge, and act as single-atom catalysts where carbon atoms stabilize the attachment of Ni adatoms. This consequently promotes the addition of carbon atoms in the edge formation. Based on our calculations we propose that, even though the range of temperatures in our experiments is different, the formation of graphene domains follows the same trends.

C. Growth of 1-LG on Ni(110)

Although the literature discusses that C-C bonds and monolayer graphene will be formed in this 110 direction, a complete understanding of the routes leading to the formation of a stable and large area of a graphene monolayer has been elusive [1–5,13–15,38,43]. The Ni(110) surface has the lowest atomic packing density. The C deposition rate ($R_{\mathrm{Ni(110)}}$) and the surface energy for Ni(110) are the largest compared to the 111 and 100 directions. On Ni(110) with gas flows of 1000 sccm for H_2 and 100 sccm for CH_4 with rapid quenching after deposition, 1-LG was obtained at $(800 \pm 1)\,^{\circ}$C, M-LG was obtained at $(1000 \pm 1)\,^{\circ}$C and $(1100 \pm 1)\,^{\circ}$C and no carbon structure formation was observed below 790 °C (see Table I).

Films of 1-LG will be incommensurate with the Ni(110) surface and this results in Moiré patterns [13,14]. In addition, the carbon nucleation sites have different orientations, producing multiple graphene domains. As a consequence, graphene in Ni(110) is expected to have poorer quality relative to that grown on the 111 plane. The Raman spectrum in Fig. 1(f) shows a significant D-band intensity for 1-LG grown on Ni(110), while Fig. 1(e) shows a very weak D-band intensity for 1-LG grown on Ni(111). Our computer simulations suggest that the graphene monolayer formed on a perfect Ni(110) surface is not planar, but has a buckling due to the different types of C-Ni bonds. The best configuration found is shown in Fig. 5, and the energetics and structural data are shown in Table II. A complete model that describes the dynamics of 1-LG formation in Ni(110) is yet to be developed, but recent information regarding diffusion and segregation may further this effort [1,15].

D. Suggested model for carbon growth on Ni(110)

Our computer simulations results suggest that carbon atoms would preferably attach to a bridge-001 site (see Fig. 6 and Table S1 for details). The carbide formation is slightly disfavored, but only by 0.09 eV. On this plane, the energy barriers to diffuse across the surface or into the bulk are closer (0.53 eV for across and 0.72 eV for into), and we expect these two processes to be more competitive compared to the 111 case. Paths and kinetic barriers are shown in Fig. 7(c). The arrival of a second C atom creates a competition between dimer formation and isolated adsorption since they have very similar energies, as shown in Fig. 6. Trimers and tetramers are less stable than dimers and are not likely to be formed. Therefore, at the low coverage regime, the 110 face shows more balanced thermodynamics, with dimer formation, diffusion, and segregation in close competition with each other.

The incommensurability of graphene with the substrate may reinforce growth through the healing mechanism of pentagons and heptagons [31]. On the other hand, the lack of hexagonal symmetry of this face may result in graphene domains growing from different nucleation sites joining with different orientations. As a consequence, we would expect graphene with poorer quality relative to the 1-LG grown on the 111 direction. Electrical measurements should also confirm these statements about the quality of the 1-LG grown on the different Ni surfaces. However, to the best of the authors' knowledge, there are no such measurements in the literature focusing on the quality of graphene formed in each direction.

In summary, we suggest that a carbon atom on the 110 plane can diffuse across the surface or into the bulk with nearly the same likelihood because the barriers for both processes are similar. At 800 °C this balance allows the surface to have a moderate carbon concentration with enough time to order. Also the bulk should not saturate, and segregation is not likely to occur. Dimers are slightly less stable than monomers, so atomic carbon is available to diffuse into the bulk while carbon concentration is low. After reaching a threshold coverage, carbon atoms dimers will be more prevalent and graphene would grow. The symmetry of the plane does not favor the formation of highly ordered graphene. When temperature is increased (1000 °C) the reaction rate of CH_4 increases and the resulting high carbon concentration produces M-LG.

E. Growth of M-LG on Ni(100)

Epitaxial growth of 1-LG is more complicated than the previous cases due to the larger mismatch between graphene and Ni(100) surface. The C deposition rate ($R_{\mathrm{Ni(100)}}$) and the surface energy for Ni(100) are smaller compared to the 110 direction but are larger compared to the 111 direction. Our computer simulations predict that, if formed, a graphene layer on the Ni(100) surface would not remain planar, but would have a large corrugation due to the mismatch between the two structures [graphene has a honeycomb structure while the Ni(100) surface has a square symmetry]. These undulations prevent some of the carbon atoms to be directly linked to the metallic surface, as shown in Fig. 5. Theoretical simulations from the literature [72] have also obtained these undulations, which may vary in amplitude between 0.2 Å to 1.0 Å depending on the graphene position and orientation with respect to the Ni surface, and also the size of the unit cell used in the simulation. In our experiments, even though we tested different growth parameters such as temperature and gas flow, 1-LG was not obtained on Ni(100). To grasp why graphene is not formed, we need to understand better how carbon interacts with the Ni atoms at the surface when adsorbed or segregated.

We performed DFT calculations of the adsorption energy of individual carbon atoms on the 100 plane, finding that the most stable site is the hollow one (see Fig. 6 and Table S1 for details). Observing the charge density difference plots (displayed in Fig. 6) and Bader charges for the three surface planes (−0.70 for C on Ni(111), −0.83 for C on Ni(110), and −0.99 for C on Ni(100)), we can deduce that the C-Ni bonds on the 100 face are stronger and more localized than on the 111 and 110 planes. This charge localization would inhibit dimer formation, due to the fact that this new C-C bond would weaken the strong C-Ni and Ni-Ni already existing bonds. This disruption in the nickel orbitals (related to spin unpairing) would take the

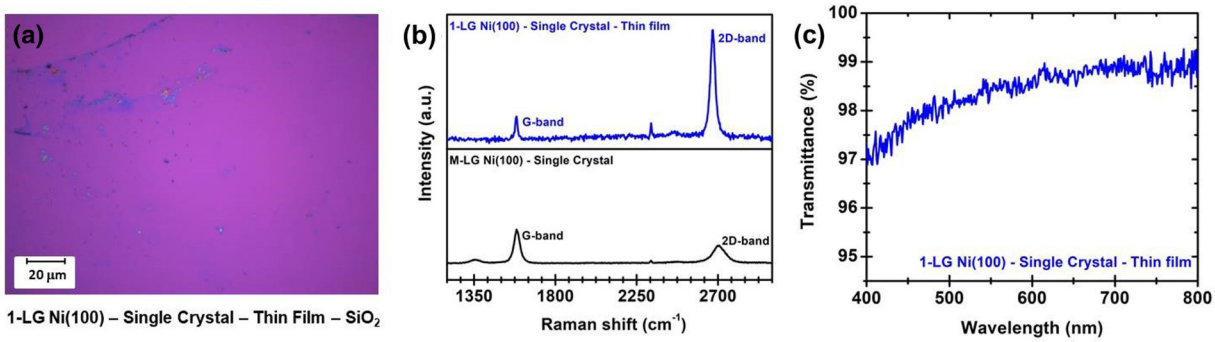

FIG. 8. (a) Optical image of the 1-LG obtained for Ni(100) films with thickness around 1mm using fast cool down approaches starting at $T = 1000\,^{\circ}$C. (b) Top: Raman spectrum of the 1-LG imaged in (a). Bottom: for comparison, the Raman spectrum of the M-LG obtained for the Ni(100) single crystal discussed in the previous section. (c) Optical transmittance across the wavelength range of 400–800 nm for 1-LG films grown from 1 mm thick Ni(100) films.

Ni crystal out of its energy minimum [1–5,28,38,40,41]. Our calculations show that the dimer formation is highly unlikely at low coverages (dimer formation is 2.38 eV higher in energy than two carbon atoms separately adsorbed), and this is also prevented by symmetry.

The large adsorption energy difference between sites (all listed in Table S1) makes lateral diffusion unlikely, with barriers in the order of 2.17 eV. Although the 100 surface is more open than the 111 plane, diffusion into the bulk is less likely in the low coverage regime (below 0.5 monolayer coverage, where C-C bonds should be disfavored) because the carbide phase with the carbon atom below the surface is very unstable (1.15 eV higher in energy than a carbon on a surface hollow site). At approximately one monolayer coverage or larger, carbon may enter the surface and create lattice disorder. Dimers are not likely to form as evidenced by prior work investigating segregation of carbon on Ni(100) surfaces that show monomers are well described by the Langmuir model where only noninteracting solute atoms are taken into account [1–5,28,38,40,41,45]. According to Porter *et al.* [1], segregation of C atoms to the surface of Ni(100) is reversible at monolayer coverages, confirming that C atoms at the surface are weakly interacting with each other.

Most theoretical predictions [1–5,9,20,30,31] point out that Ni(100) is unlikely to allow any formation of an organized carbon structure. At high carbon saturation levels, occurring at sufficiently high temperatures (above 800 °C in this work), M-LG structures are obtained on this face. Indeed, after CH_4 breaking at the 100 surface, the carbon atoms attach strongly on the hollow sites (tetracoordinated). These bonds are highly localized. Diffusion across and into is not likely to occur in the low coverage regime, because the barriers are very high. Dimers would not form, because the C-Ni bond is too strong when compared with a possible C-C bond. As the carbon concentration increases all the processes would start to compete. Some of the atoms would diffuse into the surface, and others would attach to the preexisting Ni-C layer. When saturation is reached, segregated C atom would attach to the surface carbon layer from below. The plane symmetry and the high carbon concentration (even at low temperatures) will favor the precipitation of M-LG.

F. Growth of 1-LG on Ni(100) thin films

Rasuli *et al.* [15] performed theoretical calculations simulating CVD growth of graphene on Ni(100). They predict that by varying the flux of gases and temperatures it is possible to grow high-quality monolayer graphene. In the present work, we varied the temperature up to $(1100 \pm 1)\,^{\circ}$C and varied the gas flux but we did not observe any carbon monolayer structure formation for Ni(100) single crystals. A possible explanation for predicted monolayer formation (and not multilayer formation) could be related to the fact that only four layers of Ni were used to represent the substrate, limiting a complete description of the diffusion into the substrate and segregation that might occur at these temperatures. In their calculation, strong Ni-C interactions may be underestimated at the low coverage regime, as opposed to our findings that show these are essential for predicting the formation of carbon structures using a Ni(100) catalyst.

More recently, Zou *et al.* [72] demonstrated via experiments the successful growth of 1-LG for Ni(100) single crystals and on Ni(100)-oriented domains of 1mm thick polycrystalline Ni(100). Their DFT calculations assume the interaction of a preexistent monolayer with the Ni surface and are in good agreement with ours, as briefly described above. These experiments [72] motivated us to perform experiments on 1mm-thick Ni(100) thin films. We applied the same growth conditions as for the Ni(100) single crystals, and for the same gases and flow rates ($H_2 = 1000$ sccm,$CH_4 = 100$ sccm) and growth time ($t = 5$ min). We successfully obtained 1-LG on Ni(100) films using the rapid cool-down procedure from a growth temperature of 1000 °C. Note that our results complement their findings since the growth temperature and the carbon source used here are different: their growth temperatures range from 400–600 °C and they use ethylene (C_2H_4) as a carbon source [72]. Figures 8(a)–8(c) summarize our analysis of the 1-LG obtained from 1 mm Ni(100) films, in good agreement with the analysis of the 1-LG obtained from Ni(111) and Ni(110), as discussed above.

Explaining the differences between thick and thin Ni films that lead to successful monolayer growth in thin films is an ongoing work that will be reported elsewhere. The different behavior may be because the top and bottom surfaces are no

longer isolated from one another and may mutually interact. Therefore, the energy renormalizations related to the C-Ni and Ni-Ni bonds would no longer be local. This could change the activation energies for the diffusions into bulk and across the surface, the surface energies, and adsorption energies. Another possibility is that the total amount of carbon dissolved in the Ni film is proportional to the thickness, so less carbon would then segregate to the surface in thinner films.

G. Nonoccurrence of carbon structures at low temperatures ($T < 800\,^{\circ}$C)

For the three studied crystallographic directions, no carbon structures were grown below 790 °C with gas flow rates of 1000 sccm for H_2 and 100 sccm for CH_4 and an exposure time of 300 sec followed by rapid quenching. The lack of carbon structure formation is mainly due to the decrease in the methane reactivity rate as the temperature decreases. A decrease in temperature of about 200 °C results in the decrease of CH_4 reactivity by more than an order of magnitude [26]. One way to overcome this decreased reactivity would be to increase the exposure time (or equivalently, to increase the concentration of CH_4). The use of other hydrocarbons for graphene growth at temperatures lower than 800 °C on Ni has been reported by several authors [13,14,46,47]. Even though diffusion into the bulk, diffusion across the surface, and segregation also dramatically decrease below 790 °C, we do not believe that this limits the growth, since these processes have been observed to occur at temperatures as low as 350 °C. [1,16]

IV. CONCLUSIONS

In this combined experimental-theoretical study, we have demonstrated that Ni(111) and Ni(110) can be efficiently used to grow single-layer graphene (1-LG) under ambient pressure CVD over areas on the order of a few cm^2. Upon transferring the films to dielectric substrates, our measurements confirm the presence of 1-LG on Ni(111) and Ni(110). Using the same gas flow rates and growth times, different temperatures are needed to grow 1-LG on Ni(111) [$T = (1000 \pm 1)\,^{\circ}$C] and on Ni(110) [$T = (800 \pm 1)\,^{\circ}$C]. We have also performed DFT calculations to suggest atomistic models to explain the growth of graphene on the different low-index surfaces. We propose that crystal symmetry, adsorption energies, diffusion across, diffusion into, segregation, and dimer formation are the key factors needed to formulate a description of the first stages of graphene growth. For Ni(100) the formation of 1-LG is not favored by symmetry and is also adversely affected by the very strong and localized Ni-C bonds that inhibit C-C dimer formation. However, we show that M-LG can be formed on Ni(100), in disagreement with previous predictions suggesting that organized carbon structures on Ni(100) were unlikely or not possible. Therefore our discussion is very relevant to current research efforts in graphene fabrication and applications, especially when low-temperature growth is desirable. Although only M-LG was obtained on Ni(100) single crystals, 1-LG was obtained for 1 mm thick thin films, complementing recent results by Zou *et al.* [72]. Due to the ease of multilayer growth on Ni, this study shows promise for extension to control the number of layers formed on different Ni surfaces, an added benefit for different technological applications.

ACKNOWLEDGMENTS

This research was supported by the Center for Excitonics, an Energy Frontier Research Center funded by the US Department of Energy, Office of Science, Basic Energy Sciences (BES), under Award No. DE-SC0001088. P.T.A. gratefully acknowledges support from the College of Arts and Sciences at the University of Alabama. K.K.K. acknowledges support from the National Research Foundation of Korea (NRF) grant funded by the Korea government (MSIT) (No. 2018R1A2B2002302). M.S.D. acknowledges US National Science Foundation Grant No. DMR-1507806. Computational resources were provided by Universidade Federal do ABC. F.N.R. and J.O.-A. thank FAPESP and CONICET for financial support.

[1] J. M. Blakely, J. S. Kim, and H. C. Potter, Segregation of carbon to the (100) surface of nickel, J. Appl. Phys. **41**, 2693 (1970).

[2] L. C. Isett and J. M. Blakely, Binding energies of carbon to Ni(100) from equilibrium segregation studies, Surf. Sci. **47**, 645 (1975).

[3] L. C. Isett and J. M. Blakely, Segregation isosteres for carbon at the (100) surface of nickel, Surf. Sci. **58**, 397 (1976).

[4] F. C. Schouten, O. L. J. Gijzeman, and G. A. Bootsma, Interaction of methane with Ni(111) and Ni(100); diffusion of carbon into nickel through the (100) surface; an AES-LEED study, Surf. Sci. **87**, 1 (1979).

[5] J. C. Shelton, H. R. Patil, and J. M. Blakely, Equilibrium segregation of carbon to a nickel (111) surface: A surface phase transition, Surf. Sci. **43**, 493 (1974).

[6] X. Li, W. Cai, L. Colombo, and R. S. Ruoff, Evolution of graphene growth on Ni and Cu by carbon isotope labeling, Nano lett. **9**, 4268 (2009).

[7] Q. Yu, J. Lian, S. Siriponglert, H. Li, Y. P. Chen, and S.-S. Pei, Graphene segregated on Ni surfaces and transferred to insulators, Appl. Phys. Lett. **93**, 113103 (2008).

[8] D. J. Siegel, and J. C. Hamilton, Computational study of carbon segregation and diffusion within a nickel grain boundary, Acta Macterialia **53**, 87 (2005).

[9] S. M. Kozlov, F. Vines, and A. Goerling, Bonding mechanisms of graphene on metal surfaces, J. Phys. Chem. C **116**, 7360 (2011).

[10] C. Cepek, A. Goldoni, and S. Modesti, Chemisorption and fragmentation of C60 on Pt(111) and Ni(110), Phys. Rev. B **53**, 7466 (1996).

[11] S. M. Foiles, M. I. Baskes, and M. S. Daw, Embedded-atom-method functions for the fcc metals Cu, Ag, Au, Ni, Pd, Pt, and their Alloys, Phys. Rev. B **33**, 7983 (1986).

[12] S. M. Foiles, Calculation of the surface segregation of Ni-Cu alloys with the use of the embedded-atom method, Phys. Rev. B **32**, 7685 (1985).

[13] D. Usachov, A. M. Dobrotvorskii, A. Varykhalov, O. Rader, W. Gudat, A. M. Shikin, and V. K. Adamchuk, Experimental and theoretical study of the morphology of commensurate and incommensurate graphene layers on Ni single-crystal surfaces, Phys. Rev. B **78**, 085403 (2008).

[14] A. V. Fedorova, A. Yu. Varykhalovb, A. M. Dobrotvorskiia, A. G. Chikinaa, V. K. Adamchuka, and D. Yu. Usachova, Structure of graphene on the Ni(110) surface, Phys. Solid State **53**, 1952 (2011).

[15] R. Rasuli, Kh. Mostafavi, and J. Davoodi, Molecular dynamics simulation of graphene growth on Ni(100) facet by chemical vapor deposition, J. Appl. Phys. **115**, 024311 (2014).

[16] A. Ataca, and S. Ciraci, Perpendicular growth of carbon chains on graphene from first-principles, Phys. Rev. B **83**, 235417 (2011).

[17] A. Reina, X. Jia, J. Ho, D. Nezich, H. Son, V. Bulovic, M. S. Dresselhaus, and J. Kong, Large area, few-layer graphene films on arbitrary substrates by chemical vapor deposition, Nano lett. **9**, 30 (2009).

[18] L. G. De Arco, Z. Yi, A. Kumar, and Z. Chongwu, Synthesis, transfer, and devices of single- and few-layer graphene by chemical vapor deposition, Nanotechnology, IEEE Transactions **8**, 135 (2009).

[19] K. S. Kim, Y. Zhao, H. Jang, S. Y. Lee, J. M. Kim, K. S. Kim, J.-H. Ahn, P. Kim, J.-Y. Choi, and B. H. Hong, Large-scale pattern growth of graphene films for stretchable transparent electrodes, Nature (London) **457**, 706 (2009).

[20] L. C. Isett and J. M. Blakely, Binding of carbon atoms at a stepped - Ni surface, J. Vac. Sci. Technol. **12**, 237 (1975).

[21] Y. Gamo, A. Nagashima, M. Wakabayashi, M. Terai, and C. Oshima, Atomic structure of monolayer graphite formed on Ni(111), Surf. Sci. **374**, 61 (1997).

[22] S. J. Chae, F. Güneş, K. K. Kim, E. S. Kim, G. H. Han, S. M. Kim, H. Shin, S. Yoon, J. Choi, M. H. Park, C. W. Yang, D. Pribat, and Y. H. Lee, Synthesis of large-area graphene layers on poly-nickel substrate by chemical vapor deposition: Wrinkle formation, Adv. Mater. **21**, 2328 (2009).

[23] A. Reina, S. Thiele, X. Jia, S. Bhaviripudi, M. Dresselhaus, J. Schaefer, and J. Kong, Growth of large-area single- and Bi-layer graphene by controlled carbon precipitation on polycrystalline Ni surfaces, Nano Res. **2**, 509 (2009).

[24] R. R. Nair, P. Blake, A. N. Grigorenko, K. S. Novoselov, T. J. Booth, T. Stauber, N. M. R. Peres, and A. K. Geim, Fine structure constant defines visual transparency of graphene, Science **320**, 1308 (2008).

[25] H. S. Bengaard, J. K. Nørskov, J. Sehested, B. S. Clausen, L. P. Nielsen, A. M. Molenbroek, and J. R. Rostrup-Nielsen, Steam reforming and graphite formation on Ni catalysts, J. Catal. **209**, 365 (2002).

[26] T. P. Beebe, D. W. Goodman, B. D. Kay, and J. T. Yates, Kinetics of the activated dissociative adsorption of methane on the low index planes of nickel single crystal surfaces, J. Chem. Phys. **87**, 2305 (1987).

[27] J. J. Lander, H. E. Kern, and A. L. Beach, Solubility and Diffusion Coefficient of Carbon in Nickel: Reaction Rates of NickelCarbon Alloys with Barium Oxide, J. Appl. Phys. **23**, 1305 (1952).

[28] K. S. Novoselov, A. K. Geim, S. V. Morozov, D. Jiang, Y. Zhang, S. V. Dubonos, I. V. Grigorieva, and A. A. Firsov, Electric field effect in atomically thin carbon films, Science **306**, 666 (2004).

[29] M. Herbig, D. Raabe, Y. J. Li, P. Choi, S. Zaefferer, and S. Goto, Atomic-scale quantification of grain boundary segregation in nanocrystalline material, Phys. Rev. Lett. **112**, 126103 (2014).

[30] A. Zangwill and D. D. Vvedensky, Novel growth mechanism of epitaxial graphene on metals, Nanoletters **11**, 2092 (2011).

[31] V. O. Ozcelik, S. Cahangirov, and S. Ciraci, Epitaxial growth mechanisms of graphene and effects of substrates, Phys. Rev. B **85**, 235456 (2012).

[32] X. Li, W. Cai, J. An, S. Kim, J. Nah, D. Yang, R. Piner, A. Velamakanni, I. Jung, E. Tutuc, S. K. Banerjee, L. Colombo, and R. S. Ruoff, Large-area synthesis of high-quality and uniform graphene films on copper foils, Science **324**, 1312 (2009).

[33] S. Bae, H. Kim, Y. Lee, X. Xu, J.-S. Park, Y. Zheng, J. Balakrishnan, T. Lei, H. Ri Kim, Y. I. Song, Y.-J. Kim, K. S. Kim, B. Ozyilmaz, J.-H. Ahn, B. H. Hong, and S. Iijima, Roll-to-roll production of 30-inch graphene films for transparent electrodes, Nat. Nanotech. **5**, 574 (2010).

[34] S. Bhaviripudi, X. Jia, M. S. Dresselhaus, and J. Kong, Role of kinetic factors in chemical vapor deposition synthesis of uniform large area graphene using copper catalyst, Nanoletters **10**, 4128 (2010).

[35] J. Lahiri, Y. Lin, P. Bozkurt, I. I. Oleynik, and M. Batzill, An extended defect in graphene as a metallic wire, Nature Nanotechnology **5**, 326 (2010).

[36] X. Li, Y. Zhu, W. Cai, M. Borysiak, B. Han, D. Chen, R. D. Piner, L. Colombo, and R. S. Ruoff, Transfer of large-area graphene films for high-performance transparent conductive electrodes, Nanoletters **9**, 4359 (2009).

[37] L. D. Landau and E. M. Lifshitz, *Theory of Elasticity*, 3rd ed.. (Pergamon Press, Oxford, 1986).

[38] H. Chen, W. Zhu, and Z. Zhang, Contrasting Behavior of Carbon Nucleation in the Initial Stages of Graphene Epitaxial growth on Stepped Metal Surfaces, Phys. Rev. Lett. **104**, 186101 (2010).

[39] R. S. Weatherup, B. C. Bayer, R. Blume, C. Ducati, C. Baehtz, R. Schlögl, and S. Hofmann, *In Situ* characterization of alloy catalysts for low-temperature graphene growth, Nanoletters **11**, 4154 (2011).

[40] D. A. McQuarrie, *Statistical Mechanics*, 1st ed. (Harper and Row, New York, 1976).

[41] H. Wise and J. Oudar, *Materials Concepts in Surface Reactivity and Catalysis* (Dover Publications, New York, 2001).

[42] A. Gonis, A. Meike, and P. E. A. Turchi, *Properties of Complex Inorganic Solids* (Plenum, New York, US, 1996).

[43] Y. Murata, V. Petrova, B. B. Kappes, A. Ebnonnasir, I. Petrov, Y.-H. Xie, C. V. Ciobanu, and S. Kodambaka, Moiré superstructures of graphene on faceted nickel islands, ACS Nano **4**, 6509 (2010).

[44] L. Papagno and L. S. Caputi, Determination of graphitic carbon structure adsorbed on Ni(110) by surface extended energy-loss fine-structure analysis, Phys. Rev. B **29**, 1483 (1984).

[45] A. Wiltner, Ch. Linsmeier, and T. Jacob, Carbon reaction and diffusion on Ni(111), Ni(100), and Fe(110): Kinetic parameters from x-ray photoelectron spectroscopy and density functional theory analysis, J. Chem. Phys. **129**, 084704 (2008).

[46] R. Muñoz and C. Gómez-Aleixandre, Review of CVD synthesis of graphene, Chem. Vap. Deposition **19**, 297 (2013).

[47] Y. Zhang, L. Zhang, and C. Zhou, Review of chemical vapor deposition of graphene and related applications, Acc. Chem. Res. **46**, 2329 (2013).

[48] Y. Wang, Y. Zheng, X. Xu, E. Dubuisson, Q. Bao, J. Lu, and K. P. Loh, Electrochemical delamination of CVD-grown graphene film: Toward the recyclable use of copper catalyst, ACS Nano **5**, 9927 (2011).

[49] L. Gao, W. Ren, H. Xu, L. Jin, Z. Wang, T. Ma, L.-P. Ma, Z. Zhang, Q. Fu, L.-M. Peng, X. Bao, and H.-M Cheng, Repeated growth and bubbling transfer of graphene with millimetre-size single-crystal grains using platinum, Nat. Commun. **3**, 1 (2012).

[50] D. L. Mafra, T. Ming, and J. Kong, Facile graphene transfer directly to target substrates with a reusable metal catalyst, Nanoscale **7**, 14807 (2015).

[51] A. Dahal and M. Batzill, Graphene–nickel interfaces: a review, Nanoscale **6**, 2548 (2014).

[52] Z. Xu, T. Yan, G. Liu, G. Qiao, and F. Ding, Large scale atomistic simulation of single-layer graphene growth on Ni(111) surface: molecular dynamics simulation based on a new generation of carbon–metal potential, Nanoscale **8**, 921 (2016).

[53] A. Delamoreanu, C. Rabot, C. Vallee, and A. Zenasni, Wafer scale catalytic growth of graphene on nickel by solid carbon source, Carbon **66**, 48 (2014).

[54] T. Wu, X. Zhang, Q. Yuan, J. Xue, G. Lu, Z. Liu, H. Wang, H. Wang, F. Ding, Q. Yu, X. Xie, and M. Jiang, Fast growth of inch-sized single-crystalline graphene from a controlled single nucleus on Cu–Ni alloys, Nature Mater. **15**, 43 (2016).

[55] J. A. Garlow, L. K. Barrett, L. Wu, K. Kisslinger, Y. Zhu, and J. F. Pulecio, Mechanisms of graphene growth by chemical vapour deposition on transition metals, Sci. Rep. **6**, 19804 (2016).

[56] C.-M. Seah, B. Vigolo, S.-P. Chai, S. Ichikawa, J. Gleize, Le F. Normand, F. Aweke, and A. R. Mohamed, Sequential synthesis of free-standing high quality bilayer graphene from recycled nickel foil, Carbon **96**, 268 (2016).

[57] Z. Ren, N. Meng, K. Shehzad, Y. Xu, S. Qu, B. Yu, and J. K. Luo, Mechanical properties of nickel-graphene composites synthesized by electrochemical deposition, Nanotechnology **26**, 065706 (2015).

[58] P. Hohenberg and W. Kohn, Inhomogeneous electron gas, Phys. Rev. **136**, B864 (1964).

[59] P. Giannozzi, S. Baroni, N. Bonini, M. Calandra, R. Car, C. Cavazzoni, D. Ceresoli, G. L. Chiarotti, M. Cococcioni, I. Dabo, A. Dal Corso, S. Fabris, G. Fratesi, S. de Gironcoli, R. Gebauer, U. Gerstmann, C. Gougoussis, A. Kokalj, M. Lazzeri, L. Martin-Samos, N. Marzari, F. Mauri, R. Mazzarello, S. Paolini, A. Pasquarello, L. Paulatto, C. Sbraccia, S. Scandolo, G. Sclauzero, A. P. Seitsonen, A. Smogunov, P. Umari, and R. M. Wentzcovitch, QUANTUM ESPRESSO: a modular and open-source software project for quantum simulations of materials, J. Phys.:Condens. Matter **21**, 395502 (2009).

[60] J. P. Perdew, K. Burke, and M. Ernzerhof, Generalized Gradient Approximation Made Simple, Phys. Rev. Lett. **77**, 3865 (1996).

[61] A. Dal Corso, Pseudopotentials periodic table: From H to Pu, Comput. Mater. Sci. **95**, 337 (2014).

[62] S. Grimme, Semiempirical GGA-type density functional constructed with a long-range dispersion correction, J. Comp. Chem. **27**, 1787 (2006).

[63] C. Kittel, *Introduction to Solid State Physics*, 8th ed. (John Wiley and Sons, New York, 2005).

[64] B.-J. Lee, J.-H. Shim, and M. I. Baskes, Semiempirical atomic potentials for the fcc metals Cu, Ag, Au, Ni, Pd, Pt, Al, and Pb based on first and second nearest-neighbor modified embedded atom method, Phys. Rev. B **68**, 144112 (2003).

[65] Y. W. Chung, *Practical Guide to Surface Science and Spectroscopy* (Academic Press, New York, 2001).

[66] F. Bianchini, L. L. Patera, M. Peressi, C. Africh, and G. Comelli, Atomic scale identification of coexisting graphene structures on Ni(111), J. Phys. Chem. Lett. **5**, 467 (2014).

[67] W. Zhao, S. M. Kozlov, O. Höfert, K. Gotterbarm, M. P. A. Lorenz, F. Viñes, C. Papp, A. Göling, and H.-P. Steinrück, Graphene on Ni(111): coexistence of different surface structures, J. Phys. Chem. Lett. **2**, 759 (2011).

[68] Y. Wang, G. Barcaro, F. R. Negreiros, T. Visart de Bocarmé, M. Moors, N. Kruse, M. Hou, and A. Fortunelli, Adsorption-induced restructuring and early stages of carbon-nanotube growth on Ni nanoparticles, Chem. Eur. J. **19**, 406 (2013).

[69] J. E. Mueller, A. C. T. van Duin, and W. A. Goddard III, Development and validation of ReaxFF reactive force field for hydrocarbon chemistry catalyzed by nickel, J. Phys. Chem. C **114**, 4939 (2010).

[70] See Supplemental Material at http://link.aps.org/supplemental/10.1103/PhysRevMaterials.2.073404 for additional information and results from the theoretical calculations performed in this work.

[71] L. L. Patera, F. Bianchini, C. Africh, C. Dri, G. Soldano, M. M. Mariscal, M. Peressi, and G. Comelli, Real-time imaging of adatom-promoted graphene growth on nickel, Science **359**, 1243 (2018).

[72] Z. Zou, V. Carnevali, M. Jugovac, L. L. Patera, A. Sala, M. Panighel, C. Cepek, G. Soldano, M. M. Mariscal, M. Peressi, G. Comelli, and C. Africh, Graphene on nickel (100) micrograins: Modulating the interface interaction by extended moiré superstructures, Carbon **130**, 441 (2018).